Laser driving and data processing concept for mobile trace gas sensing: Design and implementation

Chang Liu, Béla Tuzson, Philipp Scheidegger, Herbert Looser, Bernhard Bereiter, Manuel Graf, Morten Hundt, Oleg Aseev, Deran Maas, and Lukas Emmenegger

Citation: Review of Scientific Instruments **89**, 065107 (2018); doi: 10.1063/1.5026546
View online: https://doi.org/10.1063/1.5026546
View Table of Contents: http://aip.scitation.org/toc/rsi/89/6
Published by the American Institute of Physics

Laser driving and data processing concept for mobile trace gas sensing: Design and implementation

Chang Liu,[1] Béla Tuzson,[1,a)] Philipp Scheidegger,[1] Herbert Looser,[1,2] Bernhard Bereiter,[1] Manuel Graf,[1] Morten Hundt,[1] Oleg Aseev,[1] Deran Maas,[3] and Lukas Emmenegger[1]
[1]*Empa, Überlandstrasse 129, 8600 Dübendorf, Switzerland*
[2]*FHNW, Klosterzelgstrasse 2, 5210 Windisch, Switzerland*
[3]*ABB Switzerland Ltd., Baden-Dättwil, 5405 Baden, Switzerland*

(Received 21 February 2018; accepted 24 May 2018; published online 11 June 2018)

High precision mobile sensing of multi-species gases is greatly demanded in a wide range of applications. Although quantum cascade laser absorption spectroscopy demonstrates excellent field-deployment capabilities for gas sensing, the implementation of this measurement technique into sensor-like portable instrumentation still remains challenging. In this paper, two crucial elements, the laser driving and data acquisition electronics, are addressed. Therefore, we exploit the benefits of the time-division multiplexed intermittent continuous wave driving concept and the real-time signal pre-processing capabilities of a commercial System-on-Chip (SoC, Red Pitaya). We describe a re-designed current driver that offers a universal solution for operating a wide range of multi-wavelength quantum cascade laser device types and allows stacking for the purpose of multiple laser configurations. Its adaptation to the various driving situations is enabled by numerous field programmable gate array (FPGA) functionalities that were developed on the SoC, such as flexible generation of a large variety of synchronized trigger signals and digital inputs/outputs (DIOs). The same SoC is used to sample the spectroscopic signal at rates up to 125 MS/s with 14-bit resolution. Additional FPGA functionalities were implemented to enable on-board averaging of consecutive spectral scans in real-time, resulting in optimized memory bandwidth and hardware resource utilisation and autonomous system operation. Thus, we demonstrate how a cost-effective, compact, and commercial SoC can successfully be adapted to obtain a fully operational research-grade laser spectrometer. The overall system performance was examined in a spectroscopic setup by analyzing low pressure absorption features of CO_2 at 4.3 μm. *Published by AIP Publishing.* https://doi.org/10.1063/1.5026546

I. INTRODUCTION

Laser absorption spectroscopy has been proven to be a sensitive, fast, and cost-effective analytical technique and has gained widespread application in selective detection of molecular species at trace quantities.[1–3] Of special interest is the mid-infrared (MIR) region, where most of the molecular species have their fundamental ro-vibrational transitions, and thus, strong absorption features enhance the detection limit to the part-per-trillion (ppt) level.[4,5] With the rapid development and commercial availability of distributed feedback quantum cascade lasers (DFB-QCLs), the spectroscopic instrumentations achieved a high degree of field deployability. Nevertheless, there is still a significant demand for multi-compound capabilities at low cost and reduced size. A mobile laser-based gas analyzer offers new opportunities in detecting near-source emissions and investigating their spatial and temporal variability at affordable cost. To realize a compact, lightweight, and low-power solution, further developments are required for various key elements, such as photonics, laser driving, and signal processing.

With respect to photonics, many efforts have been made to design multi-wavelength QCL solutions.[6–8] Such approaches significantly reduce the amount of optical elements that are otherwise needed for beam combination.[9] Other considerable elements limiting mobile sensing applications are related to the laser driving and signal processing. Most commercial quantum cascade laser absorption spectroscopy (QCLAS)-based instruments employ either the continuous-wave (cw) or pulsed operations to drive the QCLs.[2] The cw operation offers high output power and narrow linewidth at the expense of significant power dissipation, which is generally treated by bulky heat-management and temperature control systems. Compared with the cw operation, the pulsed operation allows reducing the average power consumption but at the cost of a broader linewidth (thermal-chirp), a higher noise level due to pulse-to-pulse variations, and more expensive high-bandwidth detector and data acquisition (DAQ) devices.[10] Further variations of the above schemes were also deployed, mainly to reduce heat dissipation and obtain the Peltier temperature operation.[11,12] In all cases, the laser drivers are coupled to an external function generator, which supplies the trigger and ramp signals. Finally, the spectral data retrieval and analysis are generally implemented using a computer and multi-purpose data acquisition (DAQ) board. Therefore, the size, weight, and power consumption of such instruments can be serious limiting factors, especially for mobile sensing applications.

In this paper, we present a new design and the development of a versatile laser driver capable of operating dual-wavelength

a)Author to whom correspondence should be addressed: bela.tuzson@empa.ch

QCLs along with a compact, flexible, and powerful data processing scheme based on a System-on-Chip (SoC). Laser spectroscopic measurements are performed to demonstrate the suitability of these components for compact multi-compound gas sensing.

II. LASER DRIVING AND DATA PROCESSING CONSIDERATIONS

A. Laser driving requirements

High precision spectroscopic trace gas measurements put stringent requirements on the laser operating conditions, i.e., on the precision and stability of the driving current. Any excess noise from the laser injection current leads to temperature changes (ΔT) in the active region of the QCL and thus to a drift in its emission frequency ($\Delta\nu$). This deteriorates the spectral resolution and in severe cases induces significant bias in the concentration retrieval. The effect of the injection current on laser tuning can be inferred from Ref. 13 as $\Delta\nu/\nu = \beta_T R_{th} \Delta P$, where β_T is the temperature tuning coefficient on the order of $-(6.5 \text{ to } 9) \times 10^{-5}$ K^{-1} in the mid-IR, R_{th} is the thermal resistance of the device, and ΔP is the dissipated electrical power. The current tuning coefficient depends on both the thermal resistance and the electrical characteristics of the QCL.[14] Typical values are comprised between 0.2 and 1 MHz/μA. The impact of driving electronics noise on the spectral properties of QCLs has been investigated in detail by Tombez *et al.*[15] Estimating the laser linewidth (FWHM) as a function of the driver current noise spectral density, it was shown that a current noise lower than 1 nA/Hz$^{1/2}$ is needed to reach the intrinsic properties of QCLs.

In the context of mobile instrumentation, the heat dissipation of QCLs is another important factor. In the case of cw operation, this generally involves a bulky heat-management solution or alternatively, as mentioned earlier, a reduced duty-cycle approach can be used. Recently, in collaboration with Alpes Lasers (Switzerland), we proposed a power-efficient laser driving scheme with good noise performance opening the path toward compact packaging of cw-QCLs.[16] Although this intermittent continuous-wave (icw) driving scheme appears to be similar to quasi-cw driving,[11] i.e., allows for duty-cycle adjustment, the icw concept implements further functionalities. This leads to a compact yet a flexible laser driver that eliminates the need for any external electronics (e.g., function generator or DAQ) for current modulation while maintaining a high modulation capability (up to 20 kHz) and considerably lowering the demands on power supply performance. These characteristics are achieved by the following design: (i) a MOSFET-switch is used in combination with a large-size capacitor (10 mF) to decouple the laser driver from the external power supply during the laser operation. Hence, the laser current is exclusively provided by the charge stored in the capacitor; (ii) *RC* elements are used to adjust the current pulse profile and thus to control the wavelength tuning rate, while the resistor determines the amplitude of the laser current. Whilst these functionalities represent an added value compared to the simple quasi-cw driving, the approach has a fundamental conceptual limitation, i.e., individual laser currents cannot be freely and independently controlled, as this would require different voltage levels on the load capacitor. The situation turns more severe considering the general case of driving multiple dual-section DFB-QCLs.[17]

To overcome this limitation, we propose in this work actively controlled independent current sources for driving each QCL section. This new driver design combined with a time-division-multiplexing (TDM) scheme inherently supports the flexible driving of not only multiple QCLs but also a large variety of multi-wavelength QCL-types. However, this poses additional requirements for the driver control electronics, as discussed in Sec. III.

B. Strategy for data processing

The signal-to-noise ratio (SNR) of the spectroscopic measurement can be generally improved by rapid sampling and subsequent averaging of the spectral data. In a basic scheme, the detector signal is sampled and digitized by an analog-to-digital converter (ADC) and directly transferred to a personal computer (PC) for further data processing. In the case of rapid laser scanning (>10 kHz) at high resolution and sampling rates, this approach quickly reaches bandwidth limits for the data transfer. This can be solved by adopting real-time averaging solutions, given that the on-board synchronization of the laser current pulse and the DAQ guarantee the phase stability of the spectral data and thus prevent distortion of the averaged spectra. For this purpose, the Field Programmable Gate Array (FPGA) is the preferred solution.[18,19] Besides the possibility of implementing data processing algorithms[20] that are optimized for low memory bandwidth and hardware resource utilization, the FPGA also offers further benefits, such as high flexibility and scalability. Thus, the system inherently enables the implementation of a wide variety of different laser driving schemes, supports multiple-laser configurations, and allows for autonomous system operation.

III. HARDWARE DEVELOPMENT

A. Dual-channel QCL driver circuit

As shown in Fig. 1, there are three main features of the current source-based laser driver design. First and foremost, the driving current for each QCL is provided by an operational amplifier (OPA) based current regulator, which enables active and independent current control of each QCL. Second, a high-precision analog pulse generator is designed to generate current pulses with an adjustable amplitude, shape, and width. Third, similar to the previous design,[16] the electrical power of the driving circuit is provided by a load capacitor, which is disconnected from the external power supply during the operation of the QCL for the purpose of noise reduction. A digital trigger signal T_{load} is used to control its connection with the driving circuit through a MOSFET-switch Q_{Cload}. As the laser driving current is generated by the current regulator, it is independent of the voltage level on the load capacitor. Therefore, a small-size capacitor (e.g., 330 μF) can be used to facilitate noise and footprint reduction as well as to improve stability against thermal drifts. The icw-driver is capable to deliver a current up to 1 A for about 200 μs time duration. The circuit was also optimized for low standby-power consumption.

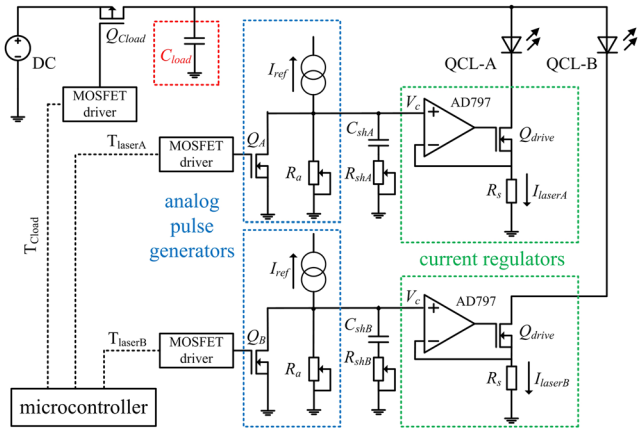

FIG. 1. Schematics of the dual-channel icw QCL current driver. An external DC power supply charges C_{load} (red). Shortly before a laser is turned on, C_{load} is disconnected from the external power supply and serves as a power source for the corresponding laser. The laser current (up to 1 A) is provided by the current regulators (green), while the amplitude and shape are defined by the settings of the analog pulse generator (blue). The temperature coefficient for all the resistors and capacitors is ±5 ppm/°C and ±25 ppm/°C, respectively. The microcontroller triggers the different phases according to the timing diagram defined by the user.

The current controller design relies on the original concept of Libbrecht and Hall.[21] The circuit was adopted to suit the relatively high compliance-voltage and currents required to drive QCLs.[22] This is a rather challenging modification as it requires a low value for R_s, and thus, the physical limit of current-noise achievable by this scheme is mainly defined by the input-referred noise floor of the operational amplifier. Therefore, an ultra-low noise (0.9 nV/Hz$^{1/2}$) operational amplifier (AD797, Analog Devices) is used to control the gate voltage of an n-channel MOSFET (Q_{drive}). The voltage drop across the sense resistor R_s (5 Ω) is set by the control voltage V_c, provided by an analog stable voltage reference.

Figure 2 schematically shows our two-stage approach to achieve high stability for I_{ref} with minimum demand on the performance of the external power supply. First, a low-dropout voltage regulator (LDO) generates a 12.5 V reference voltage, which is then used by a high side current source generator to output a stable I_{ref} of 10 mA. To generate width-, amplitude-, and shape-adjustable control voltage, a MOSFET-switch ($Q_{A/B}$), a potentiometer (R_a), and an RC-element (R_{sh} and C_{sh}) are connected in parallel to a high-precision current source of 10 mA. The pulse width is controlled by a digital trigger $T_{laserA/B}$ through the MOSFET $Q_{A/B}$.

The above circuit and driving strategy can be used in many circumstances, well beyond the exemplary implementation shown in Sec. III B. More specifically, multiple stacking of the laser drivers combined with an extended time-division-multiplexing (TDM) scheme inherently supports the flexible driving of not only multiple QCLs but also various multi-wavelength QCLs. For example, one laser channel could be used either as a pre-heating source or continuous heating source for twin-DFB-QCLs[17] and QCLs with integrated heaters (IH),[23] respectively. Similarly, Vernier QCLs can be seamlessly driven in many operating modes, when further laser-channels are involved to drive the two (front and rear) DBRs at various current levels.[24] In addition, a multitude of single- and dual-DFB QCLs of any combination or monolithically beam-combined DFB arrays[25] can in principle be driven by simply stacking additional dual-channel laser drivers. Finally, the capability to generate current pulses with various widths for individual lasers ensures high flexibility in optimizing driving conditions for each laser device.

B. FPGA-based driver control and data processing

To fully exploit the versatility of the laser driver, a flexible hardware control was required. In this context, the FPGA represents a mature technology for compact low-cost systems, which also require high reliability. The respective progress has led to many implementations also in the field of laser spectroscopy, e.g., in the form of digital lock-in amplifiers (DLIA) on FPGA platforms.[20,26,27] In this work, we take the advantage of a recently available, integrated, and open-source platform and show how to adopt this SoC (Red Pitaya[28]) for laser driver control and data processing. This system is based on a Xilinx ZYNQ-7010 processor, featuring an integrated

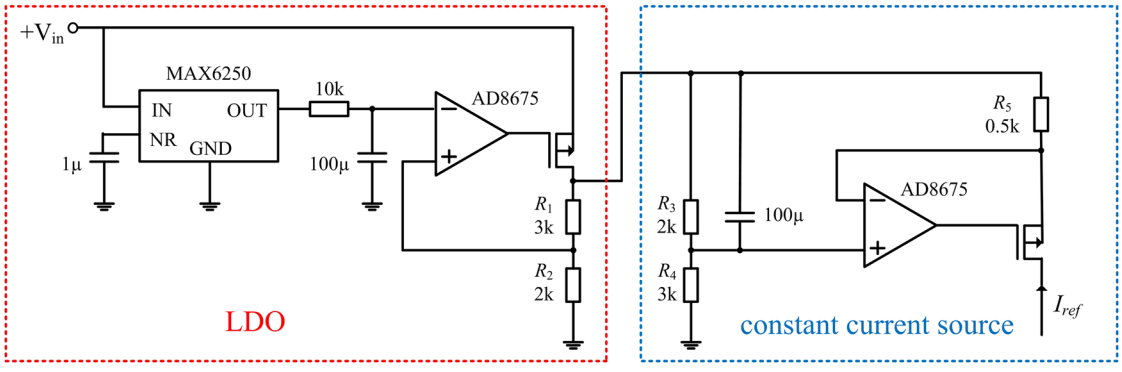

FIG. 2. Implementation of high-precision current reference I_{ref}. The low-dropout voltage regulator (LDO) uses a low-noise, precision voltage reference (MAX6250) with a 2 ppm/°C temperature coefficient. Its output noise is further reduced by a low-pass filter, which attenuates noise frequencies above its 0.16 Hz cut-off frequency. The filtered reference voltage (5 V) is fed to the inverting terminal of a low noise, rail-to-rail operational amplifier (AD8675, Analog Devices), which regulates the output voltage through a p-channel power MOSFET and feedback resistors (R_1 and R_2). The output voltage (12.5 V) serves as the power supply for the high side current regulator. The voltage across R_3 sets the reference voltage that is forced across the current sense resistor R_5 by operational amplifier's negative feedback with unity gain. Thus, a constant current of 10 mA is generated.

dual-core ARM Cortex A9 processor with Xilinx 7-series FPGA logic. The board is coupled with a dual-channel fast ADC with 14-bit resolution and a sampling rate of up to 125 MS/s. Furthermore, it provides 16 channels of programmable general purpose inputs/outputs (GPIOs).

Being an open source development platform, further functionalities can be realized by building C-based (API, Application Program Interface) routines. In addition, the Red Pitaya board can be controlled remotely over the local area network (LAN) or wireless interface using high level programming software environments via a list of commands (SCPI, Standard Commands for Programmable Instruments). These SCPI commands are recognized by the device to enable specific actions, e.g., signal generation and acquisition, digital I/O control, and communication [I^2C, Serial Peripheral Interface (SPI), universal asynchronous receiver-transmitter (UART), etc.].

The above features have been extensively used to develop and implement the functionalities described in the following paragraph. While they are not fundamentally different from previously published FPGA-based solutions, the open-source character of Red Pitaya and the generic approach described below allow rapid and efficient adaptation to a variety of applications.

The fast analog input is used to sample the detector signal, while the GPIOs provide digital triggers required for operating the dual-channel QCL driver. As schematically shown in Fig. 3, three digital triggers T_{Cload}, T_{laserA}, and T_{laserB} are generated to control the MOSFETs Q_{Cload}, Q_A, and Q_B. The widths of these trigger signals define the "ON" time of the QCLs and the connection duration of the driving circuit to the external power supply, respectively. As the same on-board clock is used for timing all the IOs and DAQs, the laser driving and data acquisition are highly synchronized on the Red Pitaya with a resolution of 8 ns. The QCLs are sequentially operated during a scan cycle, noted as W_{rep}.

As mentioned in Sec. II B, the SoC-FPGA is also used to acquire selected time windows from the detector signal including the detector background signal, i.e., W_{daq0}, and the transmission trace from each QCL, i.e., W_{daqA} and W_{daqB}, respectively. Therefore, an internal DAQ trigger, T_{DAQ}, is used in the FPGA to synchronize the data acquisition with the digital triggers for the laser driver. The number of sampling points and delay of W_{daqA} and W_{daqB} in the scan cycle can be freely selected. This operation scheme allows for multiple dual-wavelength QCLs to be driven time-multiplexed with simply adding further dual-wavelength QCL drivers and programming more GPIOs of the Red Pitaya with the similar scheme of driver control and data processing. In addition, it also allows for further data reduction, relying on the fact that usually just a fraction of the spectrum that is covered during the laser scan is relevant to calculate the target gas concentration.

As the Red Pitaya platform was mainly created to realize oscilloscope and arbitratry function generator (AFG) functionalities, it does not directly support real-time data acquisition. Therefore, it was necessary to develop and implement additional FPGA functionalities using Verilog hardware description language (HDL). The main goal was to acquire a sequence of measurements at the highest sampling rate (125 MS/s) and on each trigger accumulate these measurements on the on-chip block Random Access Memory (RAM).

In detail, the summation of the transmission data is realized using a dual-port block RAM composed in the FPGA. This has two independent ports (e.g., Port A and Port B) that enable shared access to a single memory space with the user-defined width and depth. In this work, the width and depth of the memory are defined as 32 bits and 16 384 addresses, respectively. As shown in Fig. 4, the dual-port block RAM enables simultaneous write operations to separate locations and simultaneous read operations from the same location. During a write operation, the data present at the port's input are stored in the memory at the location selected by the port's address input. During a read operation, the memory contents at the location selected by the address will appear at the port's output. In this case, Port A and Port B are used as writing and reading ports by setting EN_A and EN_B high and low, respectively. In the first scan cycle, i.e., $n = 1$, the 14-bit data sampled from the ADC are directly written into the memory on each rising edge of the clock input. From the second scan cycle, i.e., $n \geq 2$, the memory content with the ith ($i = 0, 1, \ldots, W_{daqA} + W_{daqB} - 1$) address is read out from Port B, which is used

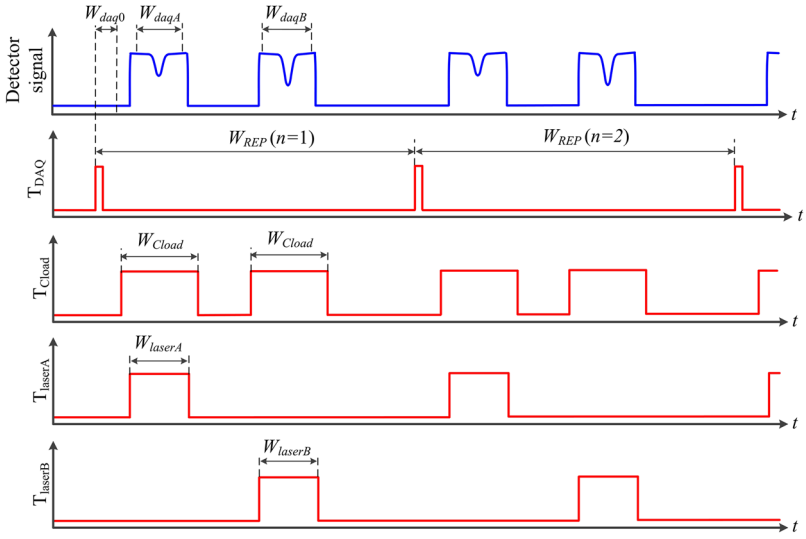

FIG. 3. Timing diagram for icw-driver control and data processing in the QCLAS measurement with a dual-wavelength QCL. The top signal shows arbitrary time window definitions for the acquired transmission spectra of two lasers. The second signal shows the cycle repetition trigger. The bottom three signals are used to operate the icw-driver.

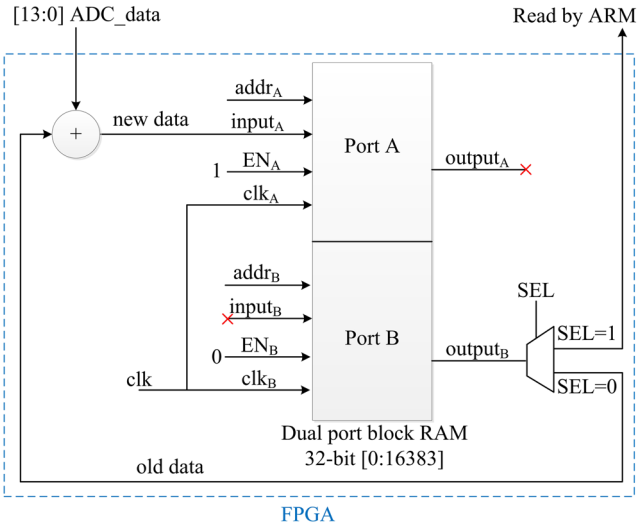

FIG. 4. Schematic diagram of the averaging function implemented on the FPGA of the Red Pitaya using Verilog HDL. This function allows real-time and on-board averaging of the transmission spectra.

to be summed with the 14-bit data newly sampled from the ADC. The summation is used as the input of Port A and written into the memory with the same address. After the last scan cycle, a multiplexer is used to switch the output of Port B from the summing loop to the ARM, where the averaged data are obtained by dividing the summed 32-bit data by N_{sum}. These data are then transferred to a remote host-PC via the TCP/IP protocol using wired/wireless connection. Optionally, the data can also be saved on a local flash drive at highest speed and without loss. This latter functionality is particularly useful in the mobile trace gas sensing to back up locally all the data in case of failed connection between the host-PC and the remote SoC.

C. Extendible functionalities for spectroscopic measurements

To facilitate the employment of the SoC for laser spectroscopy, it is also necessary to realize additional functionalities such as temperature control of the QCL, gas pressure and temperature measurement in the multi-pass cell, on-off control of valves, and other peripherals. These functionalities were implemented on the SoC using the Inter-Integrated Circuit (I^2C) bus to control additional high-precision ADC, DAC, and an IO-expander. As shown in Fig. 5, the Red Pitaya is used as the I^2C master in the standard mode (100 kbit/s), while the ADC, DAC, and IO-expander are used as the I^2C slaves. This approach provides significant expandability, as further ADCs and DACs can easily be included in the case of additional QCLs.

The temperature control of the QCL relies on the high precision thermoelectric cooler (TEC) controller (WTC3243, Wavelength Electronics, USA). A 16-bit DAC (MAX5217, Maxim Integrated) and a 24-bit ADC (LTC2493, Linear Technology) with a sampling rate of 10 S/s are used to set and read the temperature values. Other channels of the ADC are used to read gas pressure and temperature in the absorption cell as well as auxiliary temperature values. The IO-expander (TCA9555, Texas Instruments) provides additional 16-channel digital inputs/outputs (DIOs) to switch on/off valves and relays.

IV. EXPERIMENTAL

A. Hardware validation

The performance of the dual-channel laser driver is examined by evaluating its current noise characteristics. As reference, a commercial low-noise laser driver (QCL500 LAB, Wavelength Electronics, USA) is also evaluated. Both laser drivers are operated in the cw-mode at 500 mA with a 30 Ω load resistor. The voltage drop across this resistor is measured by a 24-bit digitizer (NI PXI-5922, National Instruments, USA) at a sampling rate of 15 MS/s. A large capacitor (10 mF) was used to remove the DC component so that the input range of the digitizer can be selected to its lowest level (2 $V_{pk\text{-}pk}$). The current noise power spectral density (PSD) is obtained in a post-processing step applying the fast Fourier transform (FFT) analysis method to the acquired data.

Figure 6 shows the current noise PSD of both drivers along the detection limit (0.21 nA/Hz$^{-1/2}$) of the digitizer. For the icw-driver, we estimate a current noise density of 0.74 nA/Hz$^{-1/2}$ and a rms noise performance of 0.23 μA over the bandwidth ranging from 0 to 100 kHz. The commercial driver has been found within its specification, i.e.,

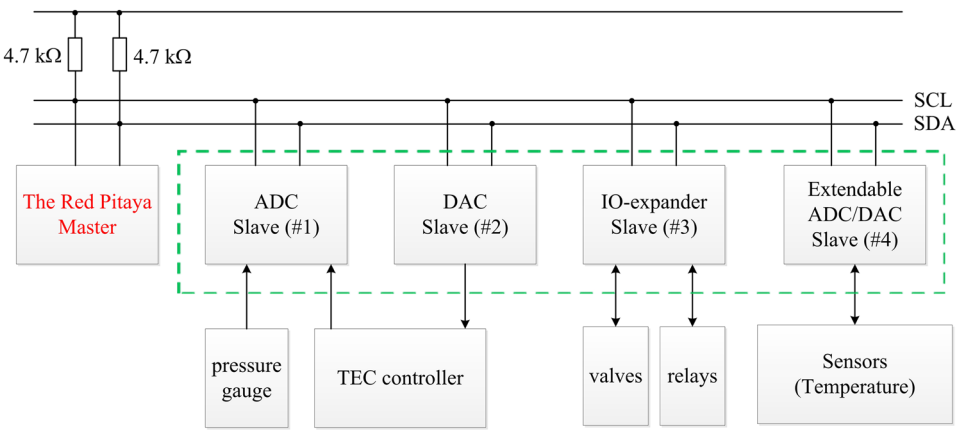

FIG. 5. Extended functionalities of the Red Pitaya SoC realized through the I^2C bus controlled custom-built high-precision ADC, DAC, and IO-expander.

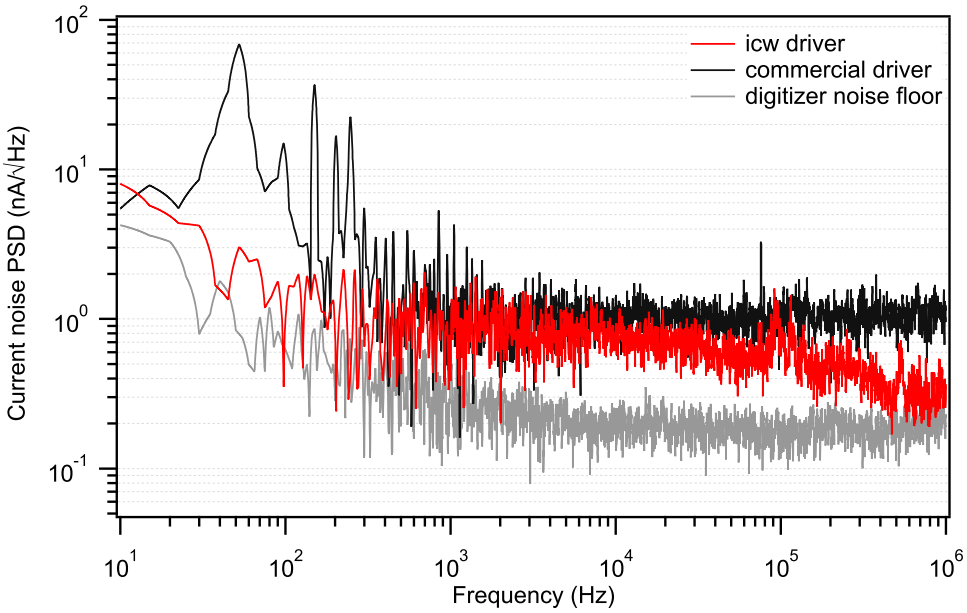

FIG. 6. Noise measurement of the icw laser driver within the bandwidth of the measurement system. The characteristic of a commercial low-noise laser driver (QCL500 LAB, Wavelength Electronics, Inc., USA) is shown as reference. Both drivers were operated at 500 mA using a 30 Ω load resistor.

1.48 nA/Hz$^{-1/2}$. As such, the dual-channel icw-driver fulfils the expectations for an ultra-low noise current source. In addition, the driver was also tested in the icw-operation mode as indicated in Fig. 3. The digitizer was triggered by T_{Cload} to the top of the current pulse. The results were similar to the values found for the cw operation mode, demonstrating that the proposed approach of icw-driving is a reliable solution.

With respect to the data acquisition, the implemented averaging function was examined by analyzing both the noise behavior and phase stability of an input signal using different numbers of consecutive scan cycles N_{sum}. The Red Pitaya was used to generate the trigger signal for the function generator, to sample at the full sampling rate of 125 MS/s, and to real-time average an artificial absorption spectrum-like waveform signal.

The measurements were performed on 16 k continuous samples recorded at a full rate of 125 MS/s. Figure 7(a) shows the sampled signal without averaging (N_{sum} = 1) and the

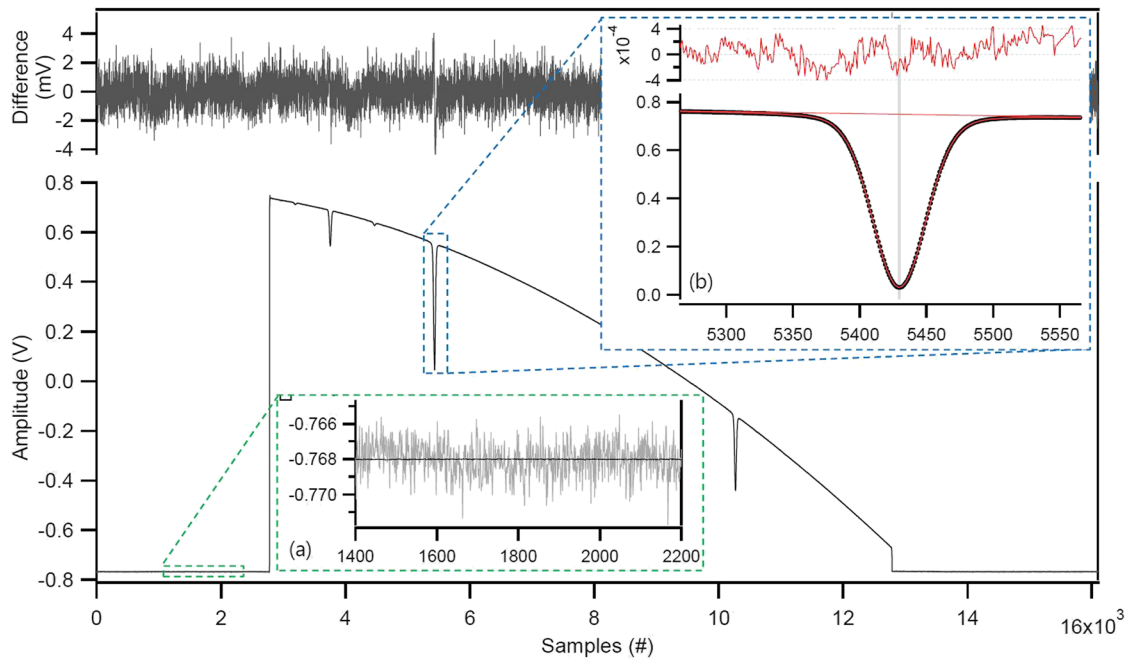

FIG. 7. Validation of the real-time averaging function implemented on the SoC by using an artificial spectrum-like waveform signal. The single-shot and the averaged (N_{sum} = 4096) spectrum, both sampled at 125 MS/s, are indicated by the gray and black traces, respectively. The difference between the two signals (top graph) has no obvious structure either at the rising/falling edge or at the flank of the "absorption signal" indicating excellent phase stability. The inset (a) shows the ADC input noise amplitude and its efficient suppression through signal averaging by the FPGA. Also the fit results of an "absorption" line of the averaged spectrum, as shown in inset (b), demonstrate that the signal averaging does not suffer from any distortion, i.e., the fit residual has no particular structure (red trace).

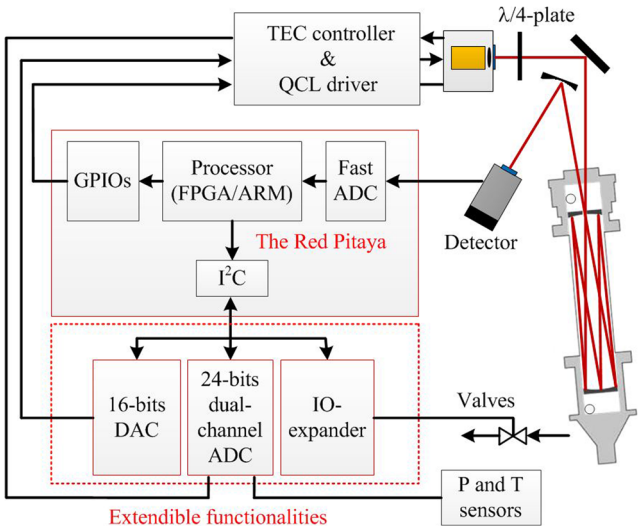

FIG. 8. Schematic diagram of the QCLAS setup used to characterize the overall performance of the developed icw-driver, the hardware control, and the data processing system.

averaged results (N_{sum} = 4096), respectively. The amplitude rms noise of 462 μV for N_{sum} = 1 decreases to about 7.38 μV for N_{sum} = 4096, which is very close to the expected 7.22 μV, assuming a purely white-noise behavior.

The phase stability was examined at the rising and falling edges of the waveform. As shown in Fig. 7, the difference between the single-shot and averaged spectrum has no particular structure at the flanks, which is a strong indication for a highly synchronized operation and properly working real-time averaging. In addition, the artificial absorption lines were fitted to a Voigt-profile to investigate potential distortions. By inspecting the fit residual (inset Fig. 7), no such issues could be observed.

B. Performance validation by QCLAS measurement

The overall performance of the developed hardware with FPGA-based driver control and SoC data processing was evaluated on a spectroscopic setup that is schematically shown in Fig. 8. The optical module was temperature stabilized at 23 ± 0.05 °C. The QCL (Alpes Lasers, Switzerland), packaged into a high heat load (HHL) with collimating optics, emits a single-mode at around 2300 cm^{-1}. The heatsink temperature of the QCL was stabilized using a TEC control loop with its input and feedback signals obtained from the I^{2}C controlled DAC and ADC. The laser was operated with a duty-cycle of 37.5% by setting the current pulse width and the repetition period to 75 μs and 200 μs, respectively. A λ/4 waveplate was placed into the beam to suppress optical feedback to the laser from the free-space optics. The collimated laser beam was then directed into an astigmatic Herriott absorption cell (AMAC-36, Aerodyne Research, Inc., USA) with an optical path of 36 m and a volume of 0.3 L. After undergoing 182 reflections, the beam exiting the absorption cell was focused onto a thermoelectrically cooled MCT detector (PVM-4TE-8, Vigo SA, Poland) with a bandwidth of 80 MHz.

To investigate the laser frequency noise figure within this spectroscopic setting, we adopted the optical frequency discriminator approach.[15,29–31] Thereby, the flank of a molecular absorption line at low pressure is used as a frequency-to-amplitude converter to investigate the laser frequency fluctuations. In our case, carbon-dioxide (CO_2) in dry atmospheric air at low pressure (5 mbar) was used.

As shown in Fig. 9, the half-height position of a CO_2 absorption line at 2302.6498 cm^{-1} was selected to achieve the highest converter response factor. The QCL was gradually tuned to the flank of the saturated absorption profile, and in the vicinity of the target position, the driving current was slightly modulated using a sinusoidal function with an amplitude of 50 μA.

This allowed finding the optimum position and verifying the linearity range. The conversion factor of the discriminator slope at this particular position has been determined to be ~10 mV/MHz. A range of about 30 MHz has been observed to present excellent linearity that guaranteed a constant frequency-to-intensity conversion. Afterwards, the laser heat-sink temperature was adjusted to fine tune the emission

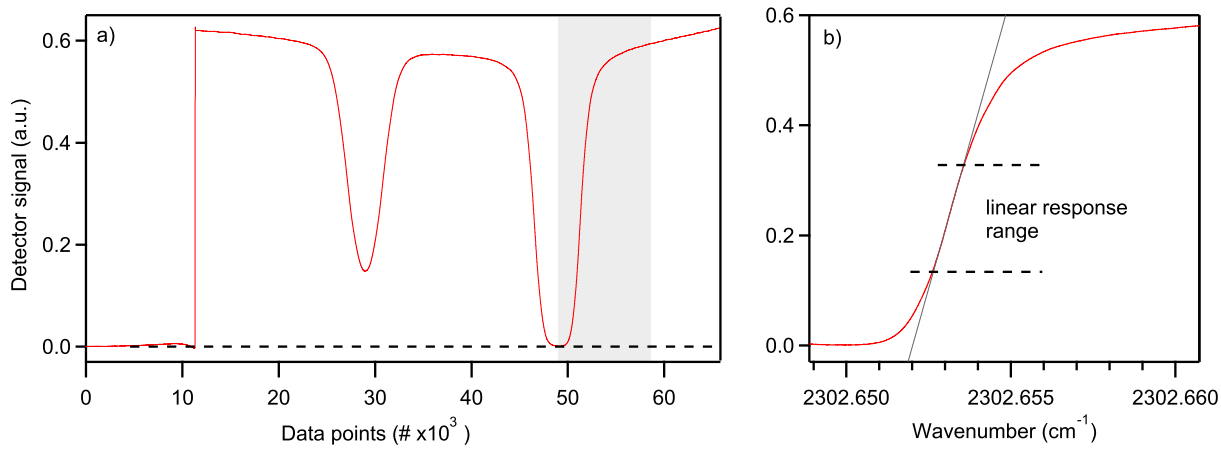

FIG. 9. Absorption spectrum of CO_2 as measured by the QCLAS setup under the experimental conditions: L = 36 m, 400 ppm CO_2, and P = 5 mbar. The shaded area indicates the region in which the intensity fluctuations were measured. The right-hand figure shows the selected absorption profile plotted versus the linearized frequency scale. The dashed lines indicate the region of the profile that is used to determine the frequency–intensity conversion factor.

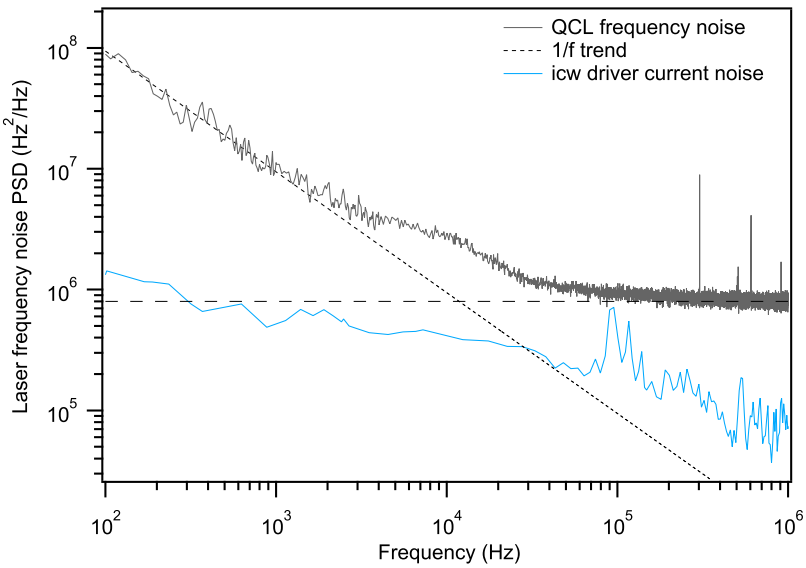

FIG. 10. Laser frequency-noise PSD. The horizontal dashed line indicates the noise floor of the detection system. For comparison, the contribution of the icw-driver current noise is also shown (blue trace).

frequency value of the laser in the middle of the linear slope and the driver was set to DC operation. The transmission signal was analyzed by a 12-bit high definition oscilloscope (Teledyne LeCroy, HDO 4045) in the spectrum analyzer mode allowing up to 72 dB of dynamic range.

The results were converted into relative frequency fluctuations of the free-running laser by using the discriminator slope value and yield the frequency-noise PSD, as shown in Fig. 10. The expected frequency-noise contributions arising from the icw-driver estimated from the current noise measurements is also plotted. From the comparison of these data, we conclude that the contribution of the current driver noise to the measured laser frequency noise has no impact on the spectral properties of QCLs. Thus, the system is fully adequate for high-precision direct absorption spectroscopic applications.

V. CONCLUSIONS

For the purpose of developing mobile multi-compound gas analyzers based on QCLs, a multi-channel icw laser driver along with real-time data processing is demonstrated. Design and validation are described in detail to allow adaptation of all components to similar instrumental designs and tasks. Relying on active current control, the icw-driver represents a versatile solution for driving multiple QCLs, incorporating low-noise operation, flexible adjustment of individual driving parameters (current amplitude, shape, and duration) as well as an improved stability against thermal drifts.

A general scheme for multi-laser driving and real-time data processing is implemented on a SoC, which combines the features of both a FPGA and an ARM processor. In the spectroscopic applications, the SoC provides the DAQ with 14-bit resolution at a sampling rate of 125 MS/s and programmable GPIOs for operating the dual-channel QCL driver, respectively. Real-time summation of the spectral data for a custom-specified number of consecutive scan cycles has been realized using the on-board FPGA of the SoC. Extended functionalities such as laser TEC control, gas pressure and temperature measurements, and control of other peripheral devices were implemented using the I^2C protocol and developing additional high precision ADC, DAC, and IO-expander.

The performance of this system was validated in terms of noise and stability on a spectroscopic setup. The laser driver unit shows comparable performance (current noise density of 0.74 $nA/Hz^{-1/2}$) with respect to commercially available low-noise drivers with the advantage of being much more compact and flexible. In combination with the SoC-based DAQ system, it fully covers all the functionalities required for an autonomous spectroscopic measurement.

ACKNOWLEDGMENTS

The authors acknowledge financial support by IRSENS 2/nanotera.ch and ABB Switzerland Ltd. The project has also received funding from the European Research Council (ERC) under the European Union's Horizon 2020 research and innovation programme [Grant Agreement No. 667507 (deepSLice)]. Further support was provided by the Swiss Commission for Technology and Innovation (CTI), the Swiss National Science Foundation (SNSF), and the Federal Office for the Environment (FOEN). The authors thank Curdin Flepp for his great engagement in the development of the I^2C functionalities to control the custom-built ADCs, DACs, and IO-expander.

[1] R. F. Curl, F. Capasso, C. Gmachl, A. A. Kosterev, B. McManus, R. Lewicki *et al.*, "Quantum cascade lasers in chemical physics," Chem. Phys. Lett. **487**, 1–18 (2010).

[2] J. B. McManus, M. S. Zahniser, D. D. Nelson, Jr., J. H. Shorter, S. Herndon, E. Wood *et al.*, "Application of quantum cascade lasers to high-precision atmospheric trace gas measurements," Opt. Eng. **49**, 111124 (2010).

[3] G. Hancock, G. Ritchie, J. P. Van Helden, R. Walker, and D. Weidmann, "Applications of midinfrared quantum cascade lasers to spectroscopy," Opt. Eng. **49**, 111121 (2010).

[4] B. Tuzson, K. Zeyer, M. Steinbacher, J. B. McManus, D. D. Nelson, M. S. Zahniser *et al.*, "Selective measurements of NO, NO_2 and NO_y in the free troposphere using quantum cascade laser spectroscopy," Atmos. Meas. Tech. **6**, 927–936 (2013).

[5]A. Fried and D. Richter, "Infrared absorption spectroscopy," *Analytical Techniques for Atmospheric Measurement* (Blackwell Publishing Ltd, Oxford, UK, 2007), pp. 72–146, ISBN:9781405123570.
[6]P. Rauter and F. Capasso, "Multi-wavelength quantum cascade laser arrays," Laser Photonics Rev. **9**, 452–477 (2015).
[7]M. Süess, R. Peretti, Y. Liang, J. Wolf, C. Bonzon, B. Hinkov *et al.*, "Advanced fabrication of single-mode and multi-wavelength MIR-QCLs," Photonics **3**, 26 (2016).
[8]C. Gmachl, A. Straub, R. Colombelli, F. Capasso, D. Sivco, A. Sergent *et al.*, "Single-mode, tunable distributed-feedback and multiple-wavelength quantum cascade lasers," IEEE J. Quantum Electron. **38**, 569–581 (2002).
[9]J. Jágerská, P. Jouy, A. Hugi, B. Tuzson, H. Looser, M. Mangold *et al.*, "Dual-wavelength quantum cascade laser for trace gas spectroscopy," Appl. Phys. Lett. **105**, 161109 (2014).
[10]G. Duxbury, N. Langford, M. T. McCulloch, and S. Wright, "Rapid passage induced population transfer and coherences in the 8 micron spectrum of nitrous oxide," Mol. Phys. **105**, 741–754 (2007).
[11]D. Weidmann, F. K. Tittel, T. Aellen, M. Beck, D. Hofstetter, J. Faist *et al.*, "Mid-infrared trace-gas sensing with a quasi- continuous-wave Peltier-cooled distributed feedback quantum cascade laser," Appl. Phys. B **79**, 907–913 (2004).
[12]A. A. Kosterev, R. F. Curl, F. K. Tittel, C. Gmachl, F. Capasso, D. L. Sivco *et al.*, "Effective utilization of quantum-cascade distributed-feedback lasers in absorption spectroscopy," Appl. Opt. **39**, 4425–4430 (2000).
[13]T. Aellen, S. Blaser, M. Beck, D. Hofstetter, J. Faist, and E. Gini, "Continuous-wave distributed-feedback quantum-cascade lasers on a Peltier cooler," Appl. Phys. Lett. **83**, 1929–1931 (2003).
[14]J. Faist, *Quantum Cascade Lasers* (Oxford University Press, United Kingdom, 2013).
[15]L. Tombez, J. Di Francesco, S. Schilt, G. Di Domenico, J. Faist, P. Thomann *et al.*, "Frequency noise of free-running 4.6 μm distributed feedback quantum cascade lasers near room temperature," Opt. Lett. **36**, 3109–3111 (2011).
[16]M. Fischer, B. Tuzson, A. Hugi, R. Brönnimann, A. Kunz, S. Blaser *et al.*, "Intermittent operation of QC-lasers for mid-IR spectroscopy with low heat dissipation: Tuning characteristics and driving electronics," Opt. Express **22**, 7014–7027 (2014).
[17]M. J. Süess, P. M. Hundt, B. Tuzson, S. Riedi, J. M. Wolf, R. Peretti *et al.*, "Dual-section DFB-QCLs for multi-species trace gas analysis," Photonics **3**, 24(2016).
[18]L. Xu, R. Xue, Y. Li, H. Zhang, and Z. Cao, "FPGA-based real-time implementation of temperature measurement via tunable diode laser absorption spectroscopy," IEEE Sens. J. **18**, 2751–2758 (2018).
[19]J. Roy, J.-D. Deschênes, S. Potvin, and J. Genest, "Continuous real-time correction and averaging for frequency comb interferometry," Opt. Express **20**, 21932–21939 (2012).
[20]A. Cifuentes and E. Marín, "Implementation of a field programmable gate array-based lock-in amplifier," Measurement **69**, 31–41 (2015).
[21]K. G. Libbrecht and J. L. Hall, "A low-noise high-speed diode laser current controller," Rev. Sci. Instrum. **64**, 2133–2135 (1993).
[22]M. S. Taubman, "Low-noise high-performance current controllers for quantum cascade lasers," Rev. Sci. Instrum. **82**, 064704 (2011).
[23]A. Bismuto, Y. Bidaux, C. Tardy, R. Terazzi, T. Gresch, J. Wolf *et al.*, "Extended tuning of mid-ir quantum cascade lasers using integrated resistive heaters," Opt. Express **23**, 29715–29722 (2015).
[24]Y. Bidaux, A. Bismuto, C. Tardy, R. Terazzi, T. Gresch, S. Blaser *et al.*, "Extended and quasi-continuous tuning of quantum cascade lasers using superstructure gratings and integrated heaters," Appl. Phys. Lett. **107**, 221108 (2015).
[25]M. Razeghi, W. Zhou, S. Slivken, Q.-Y. Lu, D. Wu, and R. McClintock, "Recent progress of quantum cascade laser research from 3 to 12 μm at the Center for Quantum Devices," Appl. Opt. **56**, H30–H44 (2017).
[26]S. G. Castillo and K. B. Ozanyan, "Field-programmable data acquisition and processing channel for optical tomography systems," Rev. Sci. Instrum. **76**, 095109 (2005).
[27]A. Chighine, E. Fisher, D. Wilson, M. Lengden, W. Johnstone, and H. McCann, "An FPGA-based lock-in detection system to enable chemical species tomography using TDLAS," in *2015 IEEE International Conference on Imaging Systems and Techniques (IST)* (IEEE, 2015), pp. 1–5.
[28]See www.redpitaya.com for S. Red Pitaya d. d.
[29]T. L. Myers, R. M. Williams, M. S. Taubman, C. Gmachl, F. Capasso, D. L. Sivco *et al.*, "Free-running frequency stability of mid-infrared quantum cascade lasers," Opt. Lett. **27**, 170–172 (2002).
[30]S. Bartalini, S. Borri, I. Galli, G. Giusfredi, D. Mazzotti, T. Edamura *et al.*, "Measuring frequency noise and intrinsic linewidth of a room-temperature DFB quantum cascade laser," Opt. Express **19**, 17996–18003 (2011).
[31]S. Bartalini, S. Borri, P. Cancio, A. Castrillo, I. Galli, G. Giusfredi *et al.*, "Observing the intrinsic linewidth of a quantum-cascade Laser: Beyond the Schawlow-Townes limit," Phys. Rev. Lett. **104**, 083904 (2010).